

Article

Effect of Urethane Crosslinking by Blocked Isocyanates with Pyrazole-Based Blocking Agents on Rheological and Mechanical Performance of Clearcoats

Young-Gun June ^{1,†}, Kevin Injoe Jung ^{1,†}, Moonhyun Choi ², Tae Hee Lee ², Seung Man Noh ^{2,*} and Hyun Wook Jung ^{1,*} 

¹ Department of Chemical and Biological Engineering, Korea University, Seoul 02841, Korea; ygjune@gmail.com (Y.-G.J.); ij@grtrkr.korea.ac.kr (K.I.J.)

² Research Center for Green Fine Chemicals, Korea Research Institute of Chemical Technology, Ulsan 44412, Korea; mhchoi89@kRICT.re.kr (M.C.); thlee@kRICT.re.kr (T.H.L.)

* Correspondence: smnoh@kRICT.re.kr (S.M.N.); hwjung@grtrkr.korea.ac.kr (H.W.J.); Tel.: +82-52-241-6070 (S.M.N.); +82-2-3290-3306 (H.W.J.)

† These authors contributed equally to this study.

Received: 12 September 2020; Accepted: 5 October 2020; Published: 7 October 2020



Abstract: A novel blocked isocyanate crosslinker was synthesized, and its applicability was investigated for the low-temperature curing of automotive clearcoats. Various pyrazole derivatives were prepared as blocking agents in isocyanate crosslinkers, which strongly affect the deblocking and curing properties of the urethane-bonded coating systems. The thermal curing properties of clearcoat samples containing a pyrazole-based blocked isocyanate crosslinker and polyol resin were characterized under two different temperature conditions (120 and 150 °C). The decrease in the amount of hydroxyl groups in the polyol before and after curing was expressed by the change in OH stretching frequency in the Fourier transform infrared (FT-IR) spectra. The real-time rheological storage moduli of the bulk clearcoat mixtures were measured via a rotational rheometer to determine the effect of pyrazole-based blocking agents on the curing dynamics. In addition, a rigid-body pendulum tester (RPT) was employed to investigate the curing behavior in the thin film form. The nano-indentation and the nano-scratch tests were conducted to examine the surface hardness and scratch resistance characteristics of the cured clearcoat films. The results show that a low-temperature curing system of clearcoats can be realized by tuning the curing temperature and reactivity of isocyanate crosslinkers blocked with pyrazole-based substituents.

Keywords: low-temperature curing; automotive clearcoat; blocked isocyanates; pyrazole blocking agents; urethane reaction; crosslinking dynamics; surface resistance

1. Introduction

Coatings for the outer surface of an automotive body have been steadily developed to improve their mechanical strength, chemical resistance, and gloss properties [1–3]. Conventional automotive coatings protect the inner frames from corrosion or physical damage and enhance the exterior aesthetics of the automotive. They consist of multiple layers, including electrocoats, primers, basecoats, and clearcoats [4–6]. Among them, the clearcoat on the top of the coating layers effectively secures the inner parts of the automotive from external damages such as those caused by acid rain etching, scratching, oxidation, staining, and bird droppings [7–9]. As the first line of defense for automotive bodies, the demand for high-quality clearcoat materials with long endurance and high performance is

increasing rapidly. In recent years, smart coating systems having self-healing [10,11], self-cleaning [12], and light-sensitive [13,14] characteristics has been explored to achieve the specialized functionality required for automotive coating systems. Therefore, it is very important to properly develop clearcoats to impart desired characteristics, which sufficiently can satisfy the current industrial and environmental standards.

In automotive original equipment manufacturer (OEM) coating processes, typical thermal curing conditions for clearcoats include curing at 150 °C for 30 min to induce the formation of a highly crosslinked coating layer [15–17]. Such curing conditions are most suitable for initiating and propagating urethane polymerization between a polyol binder and a thermal crosslinker. However, the current curing temperature is relatively high that requires excessive curing energy and process cost. The recent paradigm shift in the automotive industry with the advent of electric or autonomous vehicles has accelerated the development of lightweight automotive bodies that can withstand harsh thermal conditions [18–20]. Therefore, typical reactive clearcoat systems, based on urethane polymerization between hydroxyl (OH) groups in a polyol binder and isocyanate (NCO) groups in a crosslinker, must be improved so that they can be cured under comparatively low temperature conditions (<150 °C).

It is also mentioned that the photo-induced ultraviolet (UV) curing process for forming a clearcoat layer can be industrially implemented through the radical reaction between C=C double bonds in an acrylic resin and a photo initiator. This process offers many benefits, i.e., tunable mechanical properties, less emission of volatile organic compounds (VOCs), and a high processing speed [21–23]. However, the UV curing technology would exert a synergistic effect when accompanied with the above-mentioned thermal curing process to make up for the disadvantage that the UV light cannot completely cover the shadow regimes of curvaceous coating layers.

Automotive clearcoat systems based on urethane-bonded polymer networks via thermal curing have been widely used to fabricate cured coating layers because of their excellent properties such as resistance to solvents and other chemicals as well as outstanding stability and durability [24,25]. The blocked isocyanate (BI) crosslinker involved in such systems is typically prepared by blocking the isocyanate functionality using suitable materials (i.e., blocking agents), which prevent the active isocyanate groups from reacting with water molecules or nucleophiles [26–28]. To detach the blocking agents and subsequently commence urethane crosslinking by the exposed free isocyanate groups in the BI, sufficient thermal energy must be provided in the clearcoat.

The activation of blocked isocyanate crosslinkers and the consequent curing kinetics of crosslinked polymeric networks differ according to the chemical structure of the blocking agents. In addition, the compatibility of the blocking agents with the isocyanate groups in the crosslinker should be considered for the degree of reactivity of the urethane polymerization. For instance, phenols, oximes, and pyrazoles are well known to separate from the isocyanate group and promote a fast urethane reaction under relatively low temperature conditions [29–32]. Imidazole-based derivatives are also widely used as blocking agents for coatings because of their heterocyclic structures [33–35].

Various BIs with pyrazole-based blocking agents have been utilized in automotive clearcoats [33,34,36,37], since they undergo less yellowing and do not release toxic hazards during thermal curing process. By varying the substituents connected to the pyrazole ring, the deblocking temperature by pyrazole derivatives can be adjusted from approximately 85 to 200 °C [3,27]. Given the high curing conditions of existing automotive clearcoats (i.e., 150 °C), it is expected that the modification of BI crosslinkers using pyrazole derivatives could feasibly lower the curing temperature.

Herein, three different pyrazole derivatives were utilized as blocking agents and attached to the isocyanate groups at the ends of a hexamethylene diisocyanate (HDI) trimer crosslinker (N3300) for producing pyrazole-based BIs. The chemical structure of the substituent in the pyrazole-based blocking agents was varied to tune the deblocking behavior, which depends on the steric configuration effect of the blocking agents. The prepared thermal crosslinkers, pyrazole-based BIs, were mixed with a main binder—hydroxyl-functionalized urethane methacrylate oligomer (HFUMO) [15,16], which has hydroxyl groups on the chain. The thermally induced urethane reaction of clearcoat mixtures

containing different pyrazole-based BIs was examined from changes in the OH stretching frequency in the Fourier transform infrared (FT-IR) spectral data before and after thermal curing. The real-time crosslinking behaviors were monitored using a rotational rheometer with a heating chamber for thick clearcoat films and a rigid-body pendulum tester (RPT) for thin films. The surface mechanical properties of the fully cured clearcoat films were determined using a nano-indentation tester (NHT) and a nano-scratch tester (NST). The curing dynamics and mechanical properties of a clearcoat sample containing commercialized BI, Desmodur[®] PL350 MPA/SN (PL350), were extensively compared with those by the pyrazole-based BIs to clarify their coating applicability in the curing process of clearcoats.

2. Experimental Methods

2.1. Preparation of BIs with Pyrazole Derivatives

In first, pyrazole-based blocking agents combined with different alkyl substituents were prepared. Pyrazole (PYR) and dimethylpyrazole (DMP) were purchased from TCI Co. (Japan). Diterbutylpyrazole (DBP) was synthesized by mixing 2,2,6,6-tetramethylheptane-3,5-dione (3.0 g, 16.29 mmol, TCI Co.) and hydrazine hydrate (0.72 g, 22.80 mmol) in methanol (1.05 g, 32.55 mmol), and stirred for 1 h at room temperature. The mixture was then washed several times with distilled water. As will be discussed later, the different size of alkyl substituent in pyrazole derivatives plays an important role in the development of thermally induced crosslinking properties of clearcoats.

To produce three types of pyrazole-based BIs using PYR, DMP, and DBP, commercially provided Desmodur[®] N3300 (Covestro, Germany) with three unblocked isocyanate groups (6 g, 11.7 mmol) was treated with 5.4 mL n-butyl acetate (Sigma-Aldrich, St. Louis, MO, USA) under purged argon atmosphere, and then mixed with PYR, DMP, and DBP (6.6 g, 36.6 mmol), individually, at 35 °C for 2 h. Desmodur[®] PL350, a commercialized blocked polyisocyanate crosslinker, was also provided from Covestro (Leverkusen, Germany).

2.2. Formulation of Clearcoats Containing Pyrazole-Based BIs

The prepared pyrazole-based BIs (denoted as BI-DBP, BI-DMP, and BI-PYR) and BI-PL350 were individually mixed with the main HFUMO binder having an OH value of 125 mg KOH/g [16,17,38] (Table 1). They were mixed based on a molar ratio of 1.1:1 between the NCO group of each BI and OH group in the HFUMO. For all clearcoat samples, 1,6-hexanediol diacrylate (HDDA) was added as a diluent to decrease mixture viscosity, and BYK 306 was incorporated as a surface additive to reduce surface tension. The clearcoat samples were designated as CC-DBP, CC-DMP, CC-PYR, and CC-PL350, depending on the type of BIs. Figure 1 schematically portrays the structure of pyrazole derivatives and the urethane reaction between the BI and HFUMO polyol. After the blocking agent is dissociated from the BI under specific thermal conditions, three exposed NCO groups in the BI will react with the OH groups in the HFUMO, forming a crosslinked polymeric network.

Table 1. Formulation of clearcoats including pyrazole-based blocked isocyanates (Bis) and PL350.

Clearcoats	CC-DBP	CC-DMP	CC-PYR	CC-PL350
HFUMO (OH value = 125 KOH mg/g)			0.250 g	
BI-DBP	0.183 g			
Blocked isocyanate (BI)		0.139 g		
BI-DMP				
BI-PYR			0.124 g	
BI-PL350				0.196 g
BYK 306			0.004 g	
HDDA			0.050 g	
Total	0.487 g	0.443 g	0.428 g	0.5 g

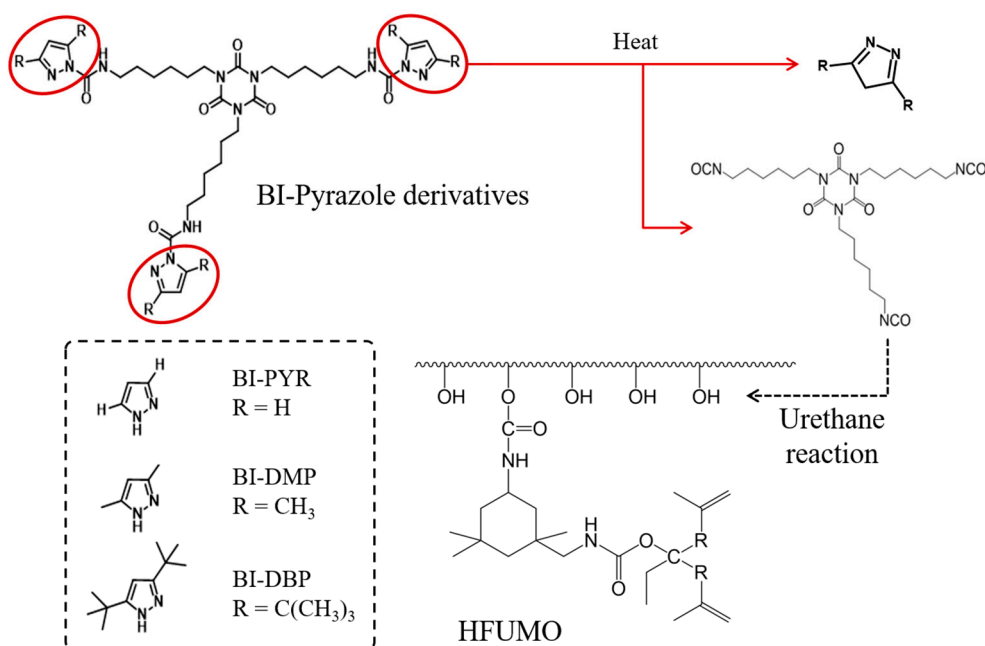


Figure 1. Scheme of the urethane reaction between various pyrazole-based BIs and hydroxyl-functionalized urethane methacrylate oligomer (HFUMO) polyol under thermal curing.

2.3. Transition of Hydroxyl Groups in HFUMO by FT-IR

To compare the urethane reactions of clearcoat samples (CC-DBP, CC-DMP, CC-PYR, and CC-PL350) considered in this study, the change in OH stretching ($3200\text{--}3700\text{ cm}^{-1}$) before and after curing under two different thermal conditions (150 and $120\text{ }^{\circ}\text{C}$) in each clearcoat sample was monitored using the attenuated total reflection mode of the FT-IR spectrometer (Spectrum Two, PerkinElmer, Waltham, MA, USA). The spectral-resolution data of 4 cm^{-1} were collected by scanning four times per clearcoat film.

2.4. Real-Time Measurement of Crosslinking Behaviors of Clearcoats

The macroscopic crosslinking evolution of clearcoat samples containing various pyrazole-based BIs was investigated in real time using a rotational rheometer (MCR-301, Anton Paar, Graz, Austria) [16,17]. Under the small-amplitude oscillatory shear mode with an angular frequency of 5 Hz and strain of 2% based on the measurement gap, the real-time storage modulus (G') was measured to clearly substantiate the growth of a crosslinked network. A parallel plate geometry with an 8 mm diameter was used, wherein the gap between the upper and lower plates was $500\text{ }\mu\text{m}$. The clearcoat sample was placed between the plates in a controlled temperature chamber (CTC). The CTC temperature was increased from $30\text{ }^{\circ}\text{C}$ to the target curing temperature of 150 or $120\text{ }^{\circ}\text{C}$ at a heating rate of 12 or $10\text{ }^{\circ}\text{C}/\text{min}$, respectively, and then maintained for 80 min .

Crosslinking features distinguished by BIs with different chemical structures in the clearcoat samples were analyzed using a rigid-body pendulum tester (RPT; RPT-3000W, A&D, Tokyo, Japan) [38,39]. During the RPT tests, a knife-shaped edge attached to an oscillating pendulum was placed on the clearcoat film of $80\text{ }\mu\text{m}$ thickness, and the real-time curing behavior was quantified in terms of the oscillatory pendulum period during the curing. The temperature was increased from 30 to $150\text{ }^{\circ}\text{C}$ or $120\text{ }^{\circ}\text{C}$ at 12 or $10\text{ }^{\circ}\text{C}/\text{min}$ heating rate, respectively, and maintained at the target temperature for 50 min .

2.5. Measurement of Surface Mechanical Properties of Fully Cured Films

The nano-indentation test (NHT3, Anton Paar Tritec SA, Corcelles-Cormondrèche, Switzerland) was conducted to evaluate the surface hardness of cured clearcoat films produced via the RPT curing

process [40,41]. The surface properties of the films were interpreted using the indentation penetration depth curves from the NHT tests, i.e., load-depth data. During the indentation test, the penetration depth created by the indenter with a 2- μm -sized Berkovich-type diamond tip was recorded along the indentation force applied on the film surface. Normal force was gradually applied at the indenter with a 20 mN/min loading rate until the maximum load of 10 mN. A 10 s pause time was assigned at the maximum load to eliminate any possible creep behavior. The indenter was unloaded at a 20 mN/min rate after the pause period. The indentation hardness (HIT) values for the films were also compared, where the detailed methodology is mentioned in previous studies [15,38,40].

The scratch features of the cured films were analyzed using an NST (Anton Paar Tritec SA, Switzerland) [41–43]. The total scratch length on the surface was 1 mm, and the normal load applied at the 2 μm sphero-conical diamond tip was gradually increased from 0.1 to 40 mN at a rate of 79.8 mN/min. The scratch resistance and pattern on the surfaces of the cured films were explained using the loads of the first critical fracture (Lc1) and scratch penetration depth profiles.

3. Results and Discussion

3.1. FT-IR Analysis on Urethane Reaction of Clearcoats with Pyrazole-Based BIs

FT-IR analysis was carried out to verify the progress of the urethane reaction between the HFUMO resin and various pyrazole-based BIs in the clearcoat films before and after thermal curing. The films were cured at 150 or 120 $^{\circ}\text{C}$ for 60 min. As shown in Figure 2, the OH stretching vibration (3200–3700 cm^{-1}) of the HFUMO in all the clearcoats significantly decreased after curing at 150 $^{\circ}\text{C}$, demonstrating that the OH groups in the HFUMO stably reacted with deblocked NCO groups in the pyrazole-based BIs at 150 $^{\circ}\text{C}$. In contrast, when the curing temperature was 120 $^{\circ}\text{C}$, the OH stretching vibration changed differently, depending on the BIs. Compared to other BIs, DBP was more detached from BI-DBP at both temperatures. This result implies that the large-sized DBP blocking agent can easily separate even below the conventional curing temperature because of the attachment of an additional electron-withdrawing group to the pyrazole ring; thus, the resulting deblocked BI can actively participate in the urethane reaction.

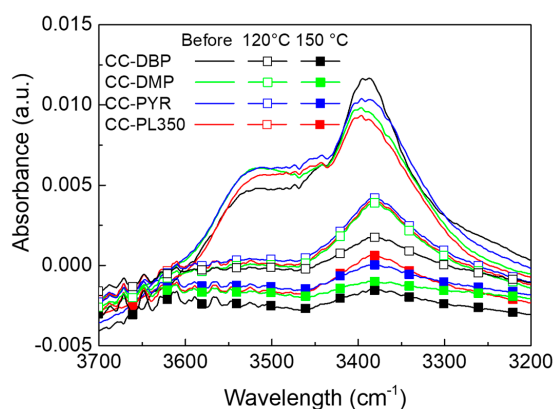


Figure 2. Changes in OH stretching vibration (3200–3700 cm^{-1}) in the HFUMO before and after thermal curing of various clearcoats at 120 and 150 $^{\circ}\text{C}$.

3.2. Real-Time Rheological Properties of Various Clearcoat Samples

The evolution of the real-time storage modulus (G') of the clearcoats under different thermal conditions (150 and 120 $^{\circ}\text{C}$) was observed using a rotational rheometer. Figure 3 shows the transient G' data of the clearcoats containing the HFUMO binder and different BIs at two curing temperatures. For thermal curing up to 150 $^{\circ}\text{C}$ (Figure 3a), the storage moduli of all clearcoat samples increased rapidly because of the extensive dissociation of pyrazole derivatives from the BIs in the high-energy state. In particular, CC-DBP was much faster crosslinked than others, followed by CC-PYR, CC-PL350,

and CC-DMP. Although the development process of G' was different for each clearcoat, the final G' value was very similar. In comparison, at a lower curing temperature of 120 °C (Figure 3b), the initiation and growth rate of crosslinking were not as rapid as in Figure 3a. CC-DBP was the only sample capable of initiating the urethane reaction within 20 min of curing time, like the Figure 3a case, while the performance of other BIs (BI-DMP, BI-PYR, and BI-PL350) was somewhat poor at a lower temperature of 120 °C. Because the DBP blocking agent has higher nucleophilic character than others caused by the bulky tertbutyl substituent, it is easily dissociated from the isocyanate groups at the given curing temperatures, resulting in an earlier initiation and a faster reaction even at a relatively lower temperature (120 °C) [27]. G' values at 90 min varied greatly depending on the type of BI. It is worth mentioning that, although the initiation of crosslinking of CC-PYR was much delayed compared to that of CC-DMP and CC-PL350 when cured at 120 °C, its reaction rate after initiation was significantly higher.

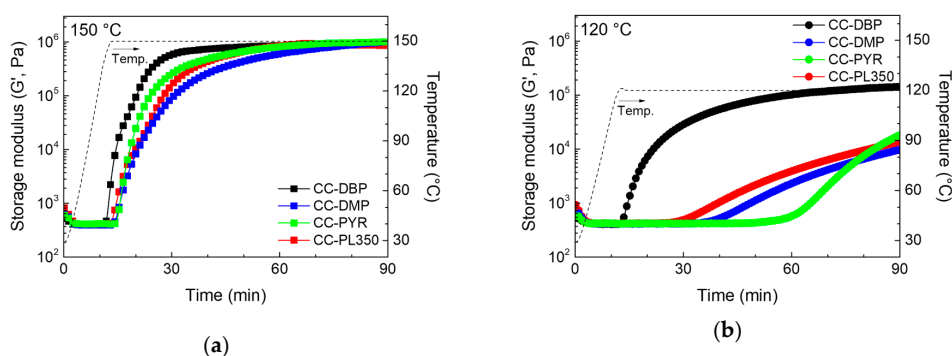


Figure 3. Real-time storage modulus data of clearcoat samples measured at two different temperatures: (a) 150 °C and (b) 120 °C.

3.3. Real-Time Oscillatory Pendulum Periods for Various Clearcoat Samples

The thermal curing behaviors of thin clearcoat films with different pyrazole-based BIs were investigated at two temperatures (150 and 120 °C) using an RPT. The oscillatory pendulum periods for the clearcoat films during thermal curing, representing the progress of network formation, are illustrated in Figure 4. At 150 °C, the curing patterns of the clearcoat samples were very analogous to those obtained by rheological measurements (Figure 4a). That is, the initiation of crosslinking and reaction rate were the highest for CC-DBP, followed by CC-PYR, CC-PL350, and CC-DMP. Figure 4b shows the pendulum periods of the samples measured at 120 °C. Compared to the rheological tests (Figure 3b), most of the clearcoats were hardly cured, except for CC-DBP because very thin films noticeably retard the reaction. Nevertheless, the crosslinking degree of CC-DBP cured at a lower temperature was obviously higher than that of the other samples.

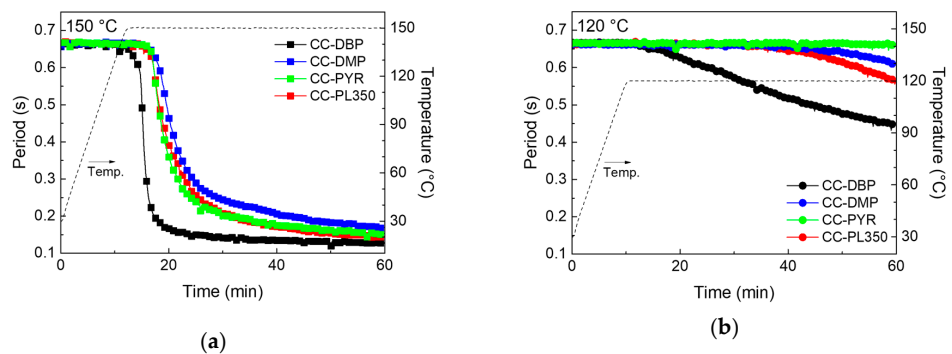


Figure 4. Rigid-body pendulum tester (RPT) results of clearcoats with various pyrazole-based BIs at curing temperatures of (a) 150 °C and (b) 120 °C.

3.4. Indentation Penetration Depths of Cured Clearcoat Films by NHT

The surface properties of the crosslinked films that underwent the RPT tests were predicted from nano-indentation measurements (Figure 5). The normal force versus indentation penetration depth curves indicate that the curing temperature of 150 °C was sufficiently high to fully cure all the samples, as depicted in Figure 5a. The plotted curves of the various clearcoat films are similar to one another, qualitatively agreeing with the final G' values in Figure 3a. In Figure 5b, the indentation depth profiles of the clearcoat films cured at 120 °C are clearly distinguishable depending on the type of BI. In particular, the indentation penetration depth of CC-DBP was much lower than that of the other samples at given curing temperatures, confirming that this film was highly crosslinked because of the easy deblocking feature of DBP. CC-DBP was more resistant to external forces than the other samples, followed by CC-PL350, CC-DMP, and CC-PYR.

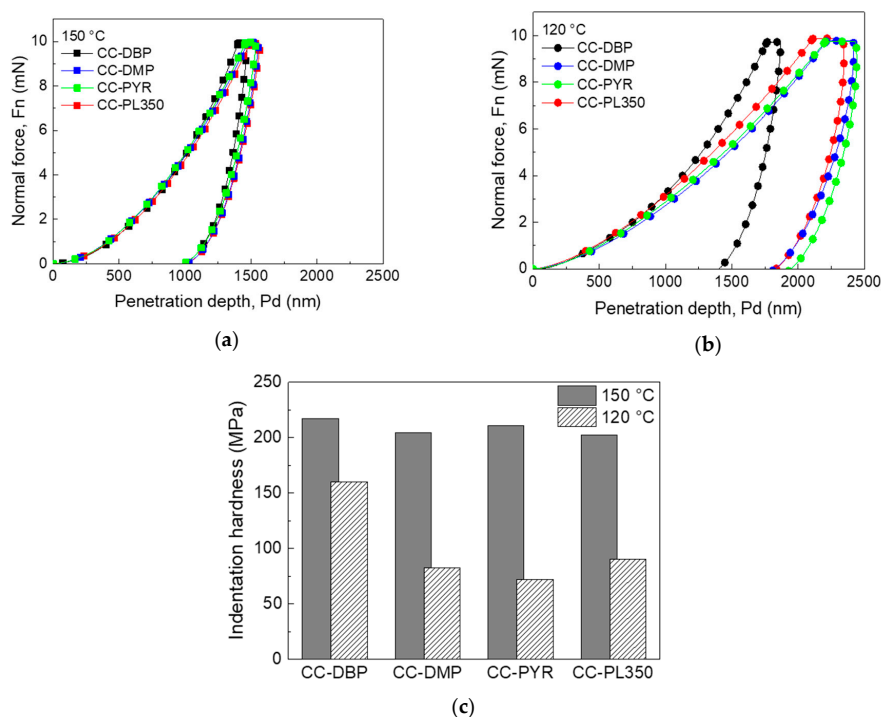


Figure 5. Indentation curves of clearcoat films having pyrazole-based BIs cured at (a) 150 °C and (b) 120 °C; (c) The indentation hardness values of clearcoat films calculated using the Oliver and Pharr method.

The HIT values, indicating the representative hardness of cured films to external forces, were calculated from the indentation depth curves, based on the Oliver and Pharr method [40], as shown in Figure 5c at two curing temperatures. The HIT values of the clearcoat films cured at 150 °C were very similar, which is in agreement with the penetration depth profiles (Figure 5a), addressing that the films were sufficiently cured. For the films cured at 120 °C, the HIT values of CC-DMP, CC-PYR, and CC-PL350 were considerably low because of the insufficient crosslinking at that temperature. However, the change in the HIT values for CC-DBP was not large, in contrast to that for other films with different BIs. Considering the excellent reactivity of BI-DBP at a temperature lower than the conventional curing temperature, which triggers the rapid growth of crosslinks, CC-DBP exhibited the highest surface hardness.

3.5. Scratch Penetration Depths of Cured Clearcoat Films by NST

Another demonstration of the surface resistance of the cured films is displayed in Figure 6 through the nano-scratch tests, which provide the scratch penetration depth profiles along the horizontal surface

of 1 mm length under the gradual vertical load condition. Figure 6a,b show the NST results of the clearcoat films cured at 150 and 120 °C, respectively. For the clearcoat films cured at 150 °C (Figure 6a), unlike the NHT results in Figure 5a, the CC-DBP film exhibited the highest scratch resistance with respect to the load, followed by CC-PYR, CC-PL350, and CC-DMP. The scratch penetration depth at 120 °C was the lowest for CC-DBP and the highest for CC-PYR. Similar to the indentation results shown in Figure 5b, BI-DBP with its bulky steric configuration favorably expedites the formation of crosslinked networks with a harder surface.

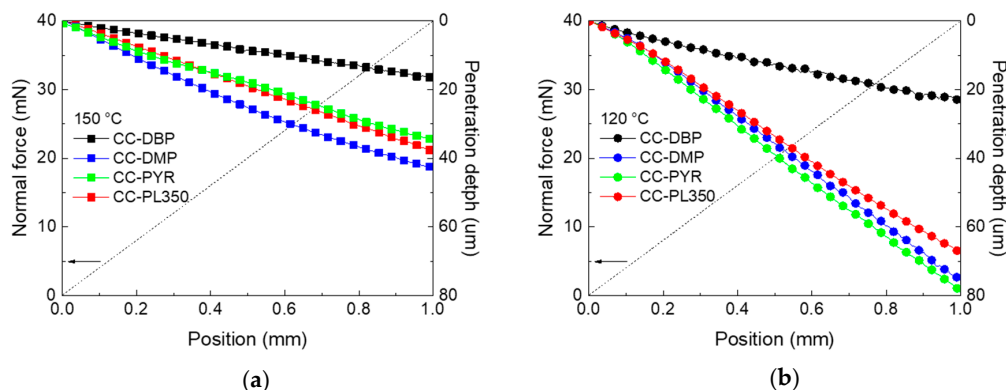


Figure 6. Penetration depth profiles of clearcoat films cured at (a) 150 °C and (b) 120 °C.

The Lc1 points on the surfaces of the clearcoat films, that is, critical loads at the first fracture, were determined from panoramic images captured after the scratch test, as shown in Figure 7. For the films cured at 150 °C, the trend for the Lc1 sequence exactly follows the indentation hardness and scratch resistance results (Figure 7a), i.e., in the order of CC-DBP, CC-PYR, CC-PL350, and CC-DMP. At a curing temperature of 120 °C, the Lc1 points were generally lower than those at 150 °C, because of the formation of insufficient crosslinking networks on the surface that could be somewhat vulnerable to external forces. However, the scratch penetration depth of the CC-DBP film became slightly lower at 120 °C than at 150 °C, demonstrating that BI-DBP would be effective in performing the crosslinking reaction of the clearcoat samples at relatively low temperatures.

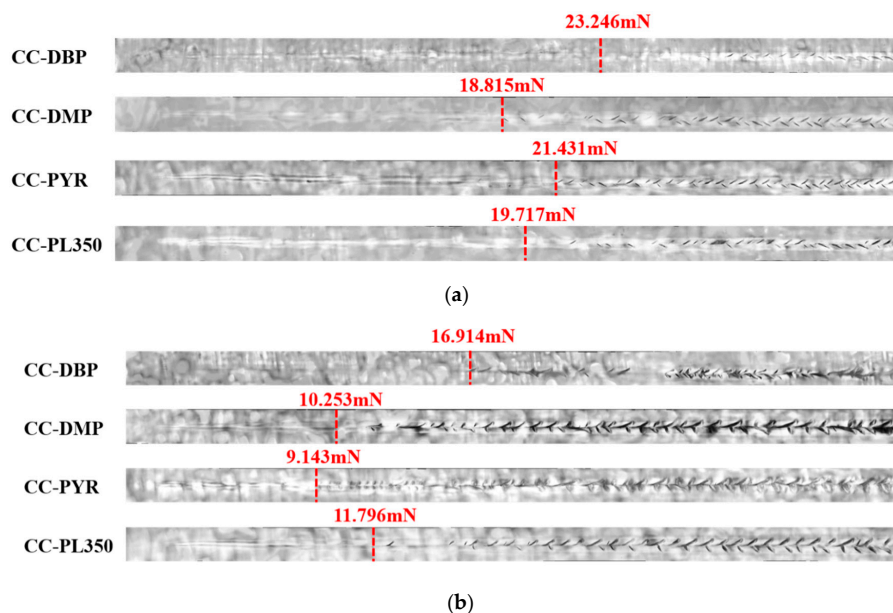


Figure 7. Scratch depth profiles and critical loads (Lc1) of clearcoat films cured at (a) 150 °C and (b) 120 °C.

4. Conclusions

The effect of pyrazole-based blocking agents (DBP, DMP, and PYR) attached to the isocyanate groups of the thermal crosslinker on the crosslinking characteristics of clearcoats was investigated through FT-IR analysis, real-time rheology and RPT, and post-curing mechanical tests. The structure of the pyrazole derivatives and the curing temperature significantly affected their dissociation performance when they were blocked to the HDI-based isocyanate crosslinker. The transition in the OH groups in the HFUMO resin before and after thermal curing was clearly confirmed from the change in OH stretching frequency from the FT-IR spectra. DBP was found to be considerably dissociated from BI-DBP, even at a lower temperature in contrast to other blocking agents, mainly caused by its bulky steric configuration. The storage moduli and oscillatory pendulum periods, which represent real-time crosslinking dynamics of thick and thin clearcoat films, respectively, demonstrated that the blocking agent with a bulkier structure, DBP in this case, was easily dissociated at given curing temperatures, promoting a higher curing rate; onset and growth rate of crosslinking were the fastest for CC-DBP, followed by CC-PYR, CC-PL350, and CC-DMP at 150 °C and CC-PL350, CC-DMP, and CC-PYR at 120 °C. The surface hardness and scratch resistance of the cured clearcoat films were also higher for the sample containing the blocking agent with a larger steric configuration. That is, the CC-DBP sample showed the hardest surface mechanical properties and was significantly better than the CC-PL350 case with commercialized crosslinker. From the various thermal curing properties of the films, it can be seen that the pyrazole-based blocking agent plays an important role in effectively lowering the curing temperature and concurrently enhancing the mechanical strength of the coating layer.

Author Contributions: Conceptualization, S.M.N. and T.H.L.; methodology, Y.-G.J. and K.I.J.; validation, S.M.N. and H.W.J.; formal analysis, Y.-G.J.; investigation, M.C.; resources, M.C.; data curation, Y.-G.J.; writing—original draft preparation, Y.-G.J. and K.I.J.; writing—review and editing, K.I.J. and H.W.J.; visualization, Y.-G.J.; supervision, S.M.N. and H.W.J.; project administration, S.M.N. and H.W.J.; funding acquisition, S.M.N. and H.W.J. All authors have read and agreed to the published version of the manuscript.

Funding: This study was supported by the Ministry of Trade, Industry and Energy (MOTIE, Korea) under Industrial Technology Innovation Programs (Grant Nos. 10067706 and 20010256).

Conflicts of Interest: The authors declare no conflict of interest.

References

1. Doerre, M.; Hibbitts, L.; Patrick, G.; Akafuah, N.K. Advances in Automotive Conversion Coatings during Pretreatment of the Body Structure: A review. *Coatings* **2018**, *8*, 405. [[CrossRef](#)]
2. Kim, B.R. VOC Emissions from Automotive Painting and their Control: A review. *Environ. Eng. Res.* **2011**, *16*, 1–9. [[CrossRef](#)]
3. Rolph, M.S.; Markowska, A.L.J.; Warriner, C.N.; O'Reilly, R.K. Blocked Isocyanates: From Analytical and Experimental Considerations to Non-polyurethane Applications. *Polym. Chem.* **2016**, *7*, 7351–7364. [[CrossRef](#)]
4. Akafuah, N.K.; Poozesh, S.; Salaimah, A.; Patrick, G.; Lawler, K.; Saito, K. Evolution of the Automotive Body Coating Process—A review. *Coatings* **2016**, *6*, 24. [[CrossRef](#)]
5. Fettis, G. *Automotive Paints and Coatings*, 2nd ed.; John Wiley & Sons: Hoboken, NJ, USA, 2008.
6. Xu, Z.; Anyasodor, G.; Qin, Y. Painting of Aluminium Panels—State of the Art and Development Issues. *MATEC Web Conf.* **2015**, *21*, 05012. [[CrossRef](#)]
7. Jardret, V.; Lucas, B.N.; Oliver, W.; Ramamurthy, A.C. Scratch Durability of Automotive Clear Coatings: A Quantitative, Reliable and Robust Methodology. *J. Coat. Technol.* **2000**, *72*, 79–88. [[CrossRef](#)]
8. Gregorovich, B.V.; Hazan, I. Environmental Etch Performance, and Scratch and Mar of Automotive Clearcoats. *Prog. Org. Coat.* **1994**, *24*, 131–146. [[CrossRef](#)]
9. Stevani, C.V.; de Faria, D.L.; Porto, J.S.; Trindade, D.J.; Bechara, E.J. Mechanism of Automotive Clearcoat Damage by Dragonfly Eggs Investigated by Surface Enhanced Raman Scattering. *Polym. Degrad. Stabil.* **2000**, *68*, 61–66. [[CrossRef](#)]
10. Urban, M.W. Stratification, Stimuli-responsiveness, Self-healing, and Signaling in Polymer Networks. *Prog. Polym. Sci.* **2009**, *34*, 679–687. [[CrossRef](#)]

11. Yoon, J.A.; Kamada, J.; Koynov, K.; Mohin, J.; Nicolay, R.; Zhang, Y.; Balazs, A.C.; Kowalewski, T.; Matyjaszewski, K. Self-Healing Polymer Films Based on Thiol–Disulfide Exchange Reactions and Self-Healing Kinetics Measured Using Atomic Force Microscopy. *Macromolecules* **2011**, *45*, 142–149. [[CrossRef](#)]
12. Parkin, I.P.; Palgrave, R.G. Self-cleaning Coatings. *J. Mater. Chem.* **2005**, *15*, 1689–1695. [[CrossRef](#)]
13. Seubert, C.M. The Future of Coatings in a World of Autonomous Vehicles. *JCT CoatingsTech* **2017**, *14*, 42–46.
14. Li, Z.; Song, C.; Li, Q.; Xiang, X.; Yang, H.; Wang, X.; Gao, J. Hybrid Nanostructured Antireflection Coating by Self-Assembled Nanosphere Lithography. *Coatings* **2019**, *9*, 453. [[CrossRef](#)]
15. Weinmann, D.; Dangayach, K.; Smith, C. Amine-functional Curatives for Low Temperature Cure Epoxy Coatings. *J. Coat. Technol.* **1996**, *68*, 29–38.
16. Jung, K.I.; Kim, B.; Lee, D.G.; Lee, T.-H.; Choi, S.Y.; Kim, J.C.; Noh, S.M.; Park, Y.I.; Jung, H.W. Characteristics of Dual-curable Blocked Isocyanate with Thermal Radical Initiator for Low-temperature Curing of Automotive Coatings. *Prog. Org. Coat.* **2018**, *125*, 160–166. [[CrossRef](#)]
17. Park, S.; Hwang, J.W.; Kim, K.N.; Lee, G.S.; Nam, J.H.; Noh, S.M.; Jung, H.W. Rheology and Curing Characteristics of Dual-curable Clearcoats with Hydroxyl Functionalized Urethane Methacrylate Oligomer: Effect of Blocked Isocyanate Thermal Crosslinkers. *Korea-Aust. Rheol. J.* **2014**, *26*, 159–167. [[CrossRef](#)]
18. Cantor, B.; Grant, P.; Johnston, C. *Automotive Engineering: Lightweight, Functional, and Novel Materials*, 1st ed.; CRC Press: Boca Raton, FL, USA, 2008.
19. Kim, D.; Lee, D.G.; Kim, J.C.; Lim, C.S.; Kong, N.S.; Kim, J.H.; Jung, H.W.; Noh, S.M.; Park, Y.I. Effect of Molecular Weight of Polyurethane Toughening Agent on Adhesive Strength and Rheological Characteristics of Automotive Structural Adhesives. *Int. J. Adhes. Adhes.* **2017**, *74*, 21–27. [[CrossRef](#)]
20. Ghassemieh, E. Materials in Automotive Application, Atate of the Art and Prospects. In *New Trends and Developments in Automotive Industry*, 1st ed.; Chiaberge, M., Ed.; InTech: New York, NY, USA, 2011; Volume 3, pp. 365–394.
21. Hwang, J.W.; Kim, K.N.; Lee, G.S.; Nam, J.H.; Noh, S.M.; Jung, H.W. Rheology and Curing Characteristics of Dual-curable Automotive Clearcoats using Thermal Radical Initiator Derived from O-imino-isourea and Photo-initiator. *Prog. Org. Coat.* **2013**, *76*, 1666–1673. [[CrossRef](#)]
22. Noh, S.M.; Lee, J.W.; Nam, J.H.; Byun, K.H.; Park, J.M.; Jung, H.W. Dual-curing Behavior and Scratch Characteristics of Hydroxyl Functionalized Urethane Methacrylate Oligomer for Automotive Clearcoats. *Prog. Org. Coat.* **2012**, *74*, 257–269. [[CrossRef](#)]
23. Seubert, C.M.; Nichols, M.E. Epoxy Thiol Photolatent Base Clearcoats: Curing and Formulation. *J. Appl. Polym. Sci.* **2010**, *7*, 615–622. [[CrossRef](#)]
24. Chang, W.-H.; Scriven, R.L.; Peffer, J.R.; Porter, S., Jr. Advances in Polyurethane Coatings (1969 to early 1972). *Ind. Eng. Chem. Product Res. Dev.* **1973**, *12*, 278–288. [[CrossRef](#)]
25. Sharmin, E.; Zafar, F. Polyurethane: An Introduction. In *Polyurethane*, 1st ed.; Zafar, F., Sharmin, E., Eds.; Intech: Rijeka, Croatia, 2012; pp. 3–6.
26. Wicks, Z.W., Jr. Blocked Isocyanates. *Prog. Org. Coat.* **1975**, *3*, 73–99. [[CrossRef](#)]
27. Wicks, D.A.; Wicks, Z.W., Jr. Blocked Isocyanates III: Part A. Mechanisms and Chemistry. *Prog. Org. Coat.* **1999**, *36*, 148–172. [[CrossRef](#)]
28. Wicks, D.A.; Wicks, Z.W., Jr. Blocked isocyanates III: Part B: Uses and Applications of Blocked Isocyanates. *Prog. Org. Coat.* **2001**, *41*, 1–83. [[CrossRef](#)]
29. Kothandaraman, H.; Nasar, A.S. The Thermal Dissociation of Phenol-blocked Toluene Diisocyanate Crosslinkers. *Polymer* **1993**, *34*, 610–615. [[CrossRef](#)]
30. Kawase, T.; Peng, X.; Ikeno, K.; Sawada, H. Surface Modification of Glass by Oligomeric Fluoroalkylating Agents Having Oxime-blocked Isocyanate Groups. *J. Adhes. Sci. Technol.* **2001**, *15*, 1305–1322. [[CrossRef](#)]
31. Gertzmann, R.; Gürtler, C. A Catalyst System for the Formation of Amides by Reaction of Carboxylic Acids with Blocked Isocyanates. *Tetrahedron Lett.* **2005**, *46*, 6659–6662. [[CrossRef](#)]
32. Mühlebach, A. Pyrazoles—A Novel Class of Blocking Agents for Isocyanates. *J. Polym. Sci. Pol. Chem.* **1994**, *32*, 753–765. [[CrossRef](#)]
33. De Aguirre, I.; Collot, J. Isocyanates Bloques: Etude Cinétique et Thermodynamique. *Bull. Soc. Chim. Belg.* **1989**, *98*, 19–30. [[CrossRef](#)]
34. Iqbal, H.M.S.; Bhowmik, S.; Benedictus, R. Performance Evaluation of Polybenzimidazole Coating for Aerospace Application. *Prog. Org. Coat.* **2017**, *105*, 190–199. [[CrossRef](#)]

35. Nasar, A.S.; Subramani, S.; Radhakrishnan, G. Synthesis and Properties of Imidazole-blocked Diisocyanates. *Polym. Int.* **1999**, *48*, 614–620. [[CrossRef](#)]
36. Bode, S.; Enke, M.; Görls, H.; Hoepfener, S.; Weberskirch, R.; Hager, M.D.; Schubert, U.S. Blocked Isocyanates: An Efficient Tool for Post-polymerization Modification of Polymers. *Polym. Chem.* **2014**, *5*, 2574–2582. [[CrossRef](#)]
37. Rolph, M.S.; Inam, M.; O'Reilly, R.K. The Application of Blocked Isocyanate Chemistry in the Development of Tunable Thermoresponsive Crosslinkers. *Polym. Chem.* **2017**, *8*, 7229–7239. [[CrossRef](#)]
38. Hwang, J.W.; Kim, K.N.; Noh, S.M.; Jung, H.W. The Effect of Thermal Radical Initiator Derived from O-imino-isourea on Thermal Curing Characteristics and Properties of Automotive Clearcoats. *J. Coat. Technol. Res.* **2015**, *12*, 177–186. [[CrossRef](#)]
39. Chiu, H.-T.; Cheng, M.-F.; Liu, H.-Y. The Analysis of Photocuring Behavior of Polyester Acrylate by Means of Differential Photo Calorimeter (DPC) and Rigid-body Pendulum Rheometer (RPT). *Polym. Plast. Technol. Eng.* **2007**, *46*, 199–205. [[CrossRef](#)]
40. Oliver, W.C.; Pharr, G.M. An Improved Technique for Determining Hardness and Elastic Modulus using Load and Displacement Sensing Indentation Experiments. *J. Mater. Res.* **1992**, *7*, 1564–1583. [[CrossRef](#)]
41. Bertrand-Lambotte, P.; Loubet, J.L.; Verpy, C.; Pavan, S. Nano-indentation, Scratching and Atomic Force Microscopy for Evaluating the Mar Resistance of Automotive Clearcoats: Study of the Ductile Scratches. *Thin Solid Films* **2001**, *398*, 306–312. [[CrossRef](#)]
42. Lee, D.G.; Sung, S.; Oh, D.G.; Park, Y.I.; Lee, S.-H.; Kim, J.C.; Noh, S.M.; Jung, H.W. Application of Polycarbonate Diol Containing Hindered Urea to Polyurethane-based Clearcoats for Tuning of Scratch-healing Properties. *J. Coat. Technol. Res.* **2020**, *17*, 963–976. [[CrossRef](#)]
43. Noh, S.M.; Lee, J.W.; Nam, J.H.; Park, J.M.; Jung, H.W. Analysis of Scratch Characteristics of Automotive Clearcoats Containing Silane Modified Blocked Isocyanates Via Carwash and Nano-scratch tests. *Prog. Org. Coat.* **2012**, *74*, 192–203. [[CrossRef](#)]



© 2020 by the authors. Licensee MDPI, Basel, Switzerland. This article is an open access article distributed under the terms and conditions of the Creative Commons Attribution (CC BY) license (<http://creativecommons.org/licenses/by/4.0/>).